Bull. Mater. Sci., Vol. 38, No. 2, April 2015, pp. 401–407. © Indian Academy of Sciences.

HRTEM investigation of phase stability in alumina–zirconia multilayer thin films

CHANCHAL GHOSH[1,*], DIVAKAR RAMACHANDRAN[1], G BALAKRISHNAN[2], P KUPPUSAMI[3] and E MOHANDAS[1]

[1]Materials Synthesis and Structural Characterisation Division, Physical Metallurgy Group, Metallurgy and Materials Group, Indira Gandhi Centre for Atomic Research, Kalpakkam 603 102, Tamil Nadu, India
[2]Department of Physics, PERI Institute of Technology, Chennai 600 048, Tamil Nadu, India
[3]Centre for Nanoscience and Nanotechnology, Sathyabama University, Chennai 600 119, Tamil Nadu, India

MS received 3 April 2014; revised 26 June 2014

Abstract. **Phase stability of nanostructured thin films can be significantly different from the stability of the same materials in bulk form because of the increased contribution from surface and interface effects. Zirconia (ZrO_2), stabilized in tetragonal and cubic phases, is a technologically important material and is used for most high temperature applications. In literature, zirconia can be found to be stabilized in its high temperature phases down to room temperature *via* two routes, doping with divalent or trivalent cations and crystallite size controls. Apart from these, in the alumina/zirconia thin-film multilayer system, a constraining effect on the zirconia layers provides another route to stabilization of the tetragonal zirconia phase at room temperature. However, in such nanostructured geometries, at high temperatures, the small diffusion lengths involved can influence the phase stability. The present work deals with the high-resolution transmission electron microscope (HRTEM) studies of pulsed laser ablated alumina–zirconia thin-film multilayers in the as deposited state and annealed up to 1473 K at 2×10^{-5} mbar. Conventional techniques such as X-ray diffraction lack the ability to detect localized phase changes at nanometre length scales and also for the low volume fraction of newly formed phases. Cross-sectional HRTEM techniques have been successful in detecting and characterizing these interactions.**

Keywords. **Alumina + zirconia multilayers; laser ablation; high-resolution transmission electron microscopy; phase stabilization; amorphous zones.**

1. Introduction

Zirconia (ZrO_2) has attracted extensive attention among material scientists owing to its wide technological applications ranging from thermal barrier coatings[1,2] to radioactive waste immobilization matrix.[3] Zirconia possesses interesting properties such as high refractive index, high resistance to oxidation, good tribological properties, high fracture toughness, high bending strength and tensile strength, oxygen ion conductivity, low thermal conductivity and high coefficient of thermal expansion.[4]

Pure ZrO_2 exists in three structural modifications: monoclinic (m-ZrO_2), tetragonal (t-ZrO_2) and cubic (c-ZrO_2) of which the tetragonal (t-ZrO_2) phase that is stable at 1443–2643 K is important for most high temperature applications and is required to be stabilized down to room temperature.[5] Two approaches can be adopted for this purpose: (i) doping and (ii) size control. Doping zirconia with trivalent (e.g., Y and rare earth elements) or divalent (e.g., Ca, Mg) cations can partially or fully stabilize the tetragonal or cubic structure at room temperature.[6–8] The reasons can be stated as (a) the diffused metal ions replace the Zr^{4+} ions from its mean equilibrium positions and hence the *c*/*a* ratio is also getting modified. The change in the *c*/*a* axial ratio with composition for ZrO_2 doped with other binary and ternary metal oxides demonstrates the phase stability of ZrO_2.[9] And (b) also the lattice oxygen ion vacancies in ZrO_2 generate at high temperature are primarily responsible for the stabilization of the tetragonal or cubic phases at high temperatures. To accommodate the thermally generated oxygen ion vacancies, the structure of ZrO_2 changes to the one having eight-fold coordination (tetragonal or cubic). Now under reduced oxygen partial pressure the same effect can also be obtained by doping divalent or trivalent cations within the ZrO_2 lattice. The oxygen ion vacancies can be generated at room temperature *via* this mechanism as a result of charge balance which in turn stabilized the high temperature tetragonal and cubic phases down to room temperature.[10,11]

On the other hand, stabilization of tetragonal morphology at room temperature can also be achieved by reducing crystallite size of zirconia below a critical size range.[12–15] The phase stability of zirconia changes drastically with the decrease in the grain size, especially in the nano-sized regime.[16] It was reported from the first-principle calculations that the surface energy of the tetragonal phase is lower than that of monoclinic phase and a reduction in the grain

*Author for correspondence (chanchal@igcar.gov.in)

size below a critical value can stabilize the high temperature tetragonal phase at lower temperature. First-principle calculations also indicate that amorphous zirconia has the smallest surface energy and thus is thermodynamically the most stable phase and that the surface energy of cubic zirconia is greater than that of monoclinic or tetragonal polymorphs making it most unstable and difficult to synthesize.[9,17] Mathematically the role of surface energy in determining the stability of different phases in ZrO_2 can also be elaborated. The theoretical variation in the specific surface area as a function of nanocrystalline size has been shown by Shukla and Seal[10] which is determined by using the relationship

$$S = 6M/\rho R, \tag{1}$$

where M is the molecular weight, ρ the density and R the nanocrystalline size in nm.

Now for the thin film multilayers where the ZrO_2 nanocrystalline sizes are within nm range, the particles do exhibit large surface area to volume ratio and the surface free energy must also be considered along with the volume energy in determining the change in free energy for monoclinic to tetragonal phase transformation.

Garvie[12] provided a thermodynamic model for the tetragonal phase stabilization in which at the phase transition temperature

$$G_t^v + \gamma_t A_t = G_m^v + \gamma_m A_m, \tag{2}$$

where G_t^v and G_m^v are the volume free energies for the tetragonal and the monoclinic structures, respectively. γ_t and γ_m are the surface free energies (cal cm^{-2}), A_t and A_m are the specific surface areas (cm^2 mol^{-1}) of the tetragonal and the monoclinic phases, respectively.

Rearranging Equation (2)

$$G_t^v - G_m^v = \gamma_m A_m - \gamma_t A_t. \tag{3}$$

Substituting Equation (1) into Equation (3)

$$\Delta G_{m\to t}^v = \gamma_m(6M/\rho_m R) - \gamma_t(6M/\rho_t R)\,,$$

$$\Delta G_{m\to t}^v = (6M/R) * [(\gamma_m/\rho_m) - (\gamma_t/\rho_t)].$$

On the basis of the above equations it can be clearly stated that in the nm size range surface energy has a greater role in determining the phase transformational behaviour in ZrO_2. Based on the works of several researchers[18–22] the critical size of 10 nm can be obtained on the basis of thermodynamic considerations. The surface energy theory clearly suggests a critical size of 10 nm below which the high temperature tetragonal structure is thermodynamically stable at room temperature within an isolated, strain free, ZrO_2 nanolaminates.

Multilayer thin films of alumina and zirconia can be synthesized using different techniques such as plasma spraying,[23] slip casting,[24] reactive sputtering[25–28] and electron beam evaporation.[29] However, these techniques are not reliable for the deposition of the nanometre thickness layers. In the present paper a pulsed laser deposition (PLD) system with excimer laser has been used to deposit nanometre thickness thin films. The main advantages in the processing of multilayers using PLD are the production of stoichiometric films of multi-component systems and low processing temperature. Besides, by controlling the number of pulses, a fine control of film thickness can be achieved. A fast response in exploring new material systems is another unique feature of PLD compared with other deposition methods.[30,31]

Unlike CeO_2 and Y_2O_3 which form solid solutions with ZrO_2 and change the phase boundary, Al_2O_3 can alter the stability through constraint imposed by grain size.[32,33] In this paper we demonstrate the combined effect of alumina addition and its nanoscale layer thickness on the stabilization of tetragonal zirconia down to room temperature. We also discuss the formation of amorphous zones due to intermixing of Al_2O_3 and ZrO_2 and *in situ* phase separation at elevated temperature. Conventional techniques are inadequate to detect such changes at the nanometre scale. High-resolution transmission electron microscopy (HRTEM) of cross-sectional samples has been used to detect and characterize these phase transformations and intermixing of the layers. The alumina/zirconia multilayer is of interest for the development of functionally graded thermal barrier coating having high wear and oxidation resistance. The present work examines the integrity and phase stability of such multilayers in the as deposited and at high temperature annealed conditions.

2. Materials and methods

Al_2O_3/ZrO_2 multilayers were synthesized by pulsed laser deposition using KrF excimer laser ($\lambda = 248$ nm) using sintered targets of alumina and zirconia (99.99% purity) at partial pressure of oxygen of 3×10^{-3} mbar at room temperature. PLD was used to obtain the multilayers of alumina and zirconia on a Si(100) single crystal substrate with different zirconia layer thickness (15 and 7 nm) keeping the alumina thickness same (5 nm). The sintered targets used were pure α-alumina phase with a rhombohedral structure ($a = 4.75$ Å, $c = 12.99$ Å) in agreement with JCPDS data (# 46-1212) and a pure zirconia pellet that had a higher volume fraction of monoclinic and small fraction of tetragonal phase (JCPDS # 65-1025 and # 50-1089, respectively). The multilayer sample was subsequently *in situ* heat treated up to 1473 K under vacuum of 2×10^{-5} mbar in a high temperature X-ray diffractometer (INEL XRG-3000 Diffractometer) attached with position-sensitive detector and Buehler 2.4 HDK high temperature camera.[34–36]

Cross-sectional HRTEM (XTEM) of the as-deposited specimen was carried out on multilayers of alternating ~15 nm zirconia and ~5 nm alumina thin films. For XTEM of the annealed one, multilayer sample with zirconia thickness ~7 nm was selected. The experimental details of the as-deposited multilayer with 7 nm zirconia layers has already been reported somewhere else.[36]

To prepare the XTEM specimen, the multilayer samples were diced into 1 × 2 × 0.5 mm cuboids and two such pieces were glued with G1 epoxy with the nano-laminates facing each other. The whole assembly was then fitted into titanium slot grids with slot size 2 × 1.2 mm. This was thinned down mechanically to ∼30 μm and subsequently ion-milled to electron transparency in Technoorg Linda IV 4 ion miller. Enough care was taken to remove the surface damage layers induced by the high-energy ion milling by low-energy ion milling in a Technoorg Linda IV 6 Gentle Mill.

HRTEM studies were carried out in a JEOL 2000 EX II (T) transmission electron microscope having a point resolution of 0.19 nm at an operating voltage of 200 kV. The microscope was equipped with a Lheritier Multi-Scan CCD camera to record digital images from which quantitative analysis was performed. Phase identification was made from high-resolution digital images by calculating power spectra from ∼5 nm wide crystalline regions and analysing them for inter-planar spacings and angles.

3. Results and discussion

Figure 1 shows a relatively low-magnification bright-field image of the alternate layers of zirconia and alumina in cross-section, illustrating the overall nano-laminate structure. The silicon substrate and the G1 epoxy can be observed on two sides of the multilayers. The alumina layer appearing light in the image, clearly separates the polycrystalline zirconia layers, which appear dark due to higher atomic number. It can also be observed that the as-deposited multilayers are well defined, of uniform thickness over large distances and with flat interfaces in between the two phases. The thickness of the alumina and zirconia nano-laminates is observed to be 5 and 15 nm, respectively.

The inset of figure 1 shows selected area electron diffraction (SAD) pattern from the multilayer region studied above, containing both Al_2O_3 and ZrO_2 nano-layers. The rings are mostly indexed as monoclinic zirconia, while a very few are from tetragonal phase. From the ring pattern, it is clear that ZrO_2 is polycrystalline. No rings corresponding to crystalline alumina are observed, indicating that the alumina is amorphous in nature. In the as-deposited alumina/zirconia multilayer containing 7-nm-thick zirconia film, alumina is amorphous and zirconia is found to be tetragonal, which has already been reported by the authors somewhere else.[36]

Figure 2 shows the HRTEM images from both alumina and zirconia region. The alumina layers are observed to be totally amorphous in nature, while individual zirconia nanocrystallites are seen in the zirconia layers. The image shows that the size of the individual zirconia crystallites is invariably equal to, or slightly smaller than the thickness of the zirconia layer. The observed lattice structures have been analysed for spacings and angles, and individual crystallites can be identified as tetragonal or monoclinic phases of zirconia in many cases, when suitably oriented. A couple of examples are annotated on the right side of figure 2.

The lattice spacings of the zirconia nanocrystallites were determined by measuring spot positions in the power spectrum corresponding to lattice spacing in the HRTEM image. Two such calculated power spectrum has been shown in

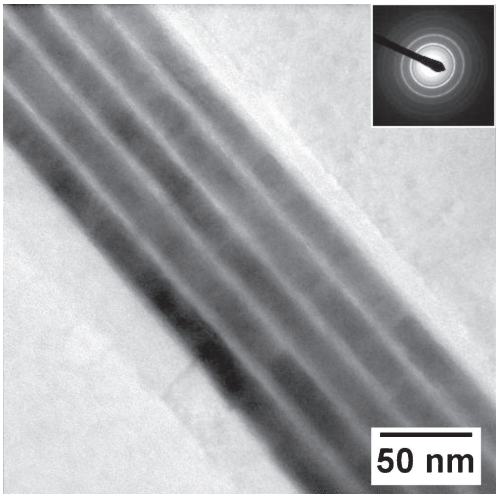

Figure 1. Low-magnification bright-field image showing multilayers of Al_2O_3 and ZrO_2. Dark bands correspond to ZrO_2 while bright bands in between are Al_2O_3 layers. Inset shows the SAD pattern from zirconia–alumina nanolaminate consisting 15-nm-thick zirconia layers. Pattern is indexed as polycrystalline mostly in monoclinic phase. No evidence for crystalline alumina is present.

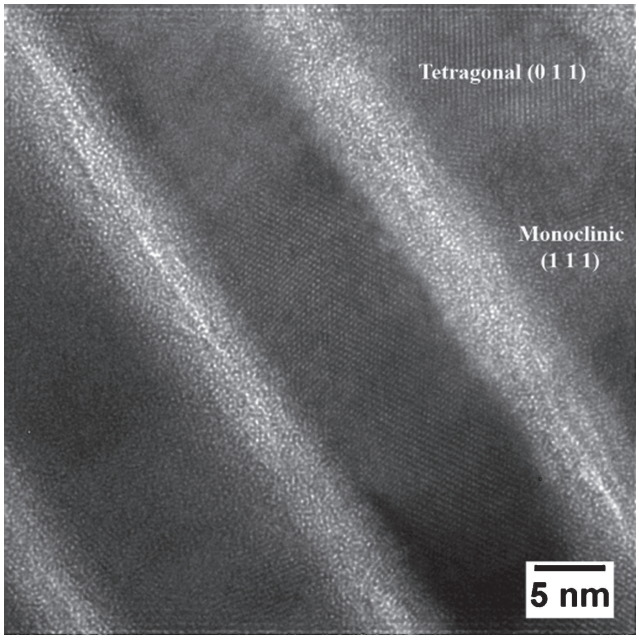

Figure 2. HRTEM of zirconia from a portion of the multilayer showing the crystalline nature with lattice spacing indexed both tetragonal and monoclinic structure. There is no evidence of crystallization from the alumina nanolayer and appear to be totally amorphous.

figure 3. They have been generated from the top left corner of the micrograph shown in figure 2 and has been indexed with (011) of tetragonal ZrO_2 and (111) of monoclinic ZrO_2. A large number of power spectrums have been analysed from the different regions of the multilayers and found that ZrO_2 is predominantly in the monoclinic structure.

Figure 4 is a relatively low-magnification bright-field micrograph of the multilayers heat-treated at 1473 K, showing the overall structures through its cross-sectional view. Here quite a large number of nano-laminates can be observed along with the silicon substrate on one side. Alumina layers are seen with higher brightness in between

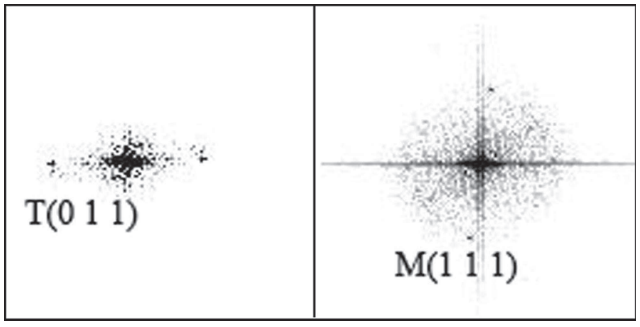

Figure 3. Power spectrum generated from the ZrO_2 nanocrystallites shown in figure 2.

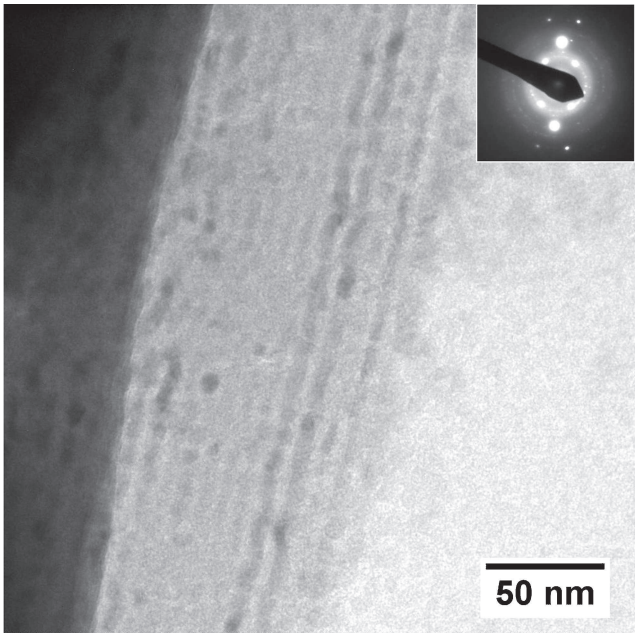

Figure 4. Low-magnification bright-field image showing the cross-sectional view of the Al_2O_3–ZrO_2 multilayers. Dark bands correspond to ZrO_2 while bright bands in between are Al_2O_3 layers. Here the layers are not well resolved at the interfaces and also they are not looking straight throughout. Inset shows SAD pattern from the same region of the multilayers, consisting 7-nm-thick zirconia layers. Pattern is indexed as polycrystalline tetragonal phase. No evidence for crystalline alumina is present.

polycrystalline zirconia layers which appear darker in the micrograph. Zirconia nano-laminates are not continuous throughout and are also seen to be distorted in some regions. Nano-layers are not well separated at the interfaces and the interfaces are also not flat. There are discontinuities in the zirconia layers where the nano-laminates cannot be identified separately. The average thickness of each of the nano-layers is measured to be ∼7 nm. Figure 4 (inset) is the SAD pattern taken from the same region of the multilayer. It shows a ring pattern, characteristic of diffraction from a polycrystalline specimen, and has been indexed as tetragonal zirconia. The additional bright spots are from the silicon substrate. No rings due to monoclinic zirconia or crystalline alumina have been observed. These results are in agreement with our other structural characterization studies on similar films reported earlier.[34–36]

Figure 5 shows high-resolution phase contrast image from the heat-treated multilayer sample. In contrast to the as-deposited multilayers, the zirconia layers are discontinuous and the interfaces between the zirconia and alumina layers are diffuse. While, most part of the multilayer structures are still evident, groups of crystallites in the zirconia layers are seen to be separated by regions which are seem to be amorphous. This region is actually amorphous and does not appear so due to grain orientation has been confirmed by tilting the specimen in different zone axis orientation. There is a bright/dark contrast difference between the zirconia and alumina layers. Alumina layers are amorphous in all regions. However, in some regions, the distinction between amorphous alumina

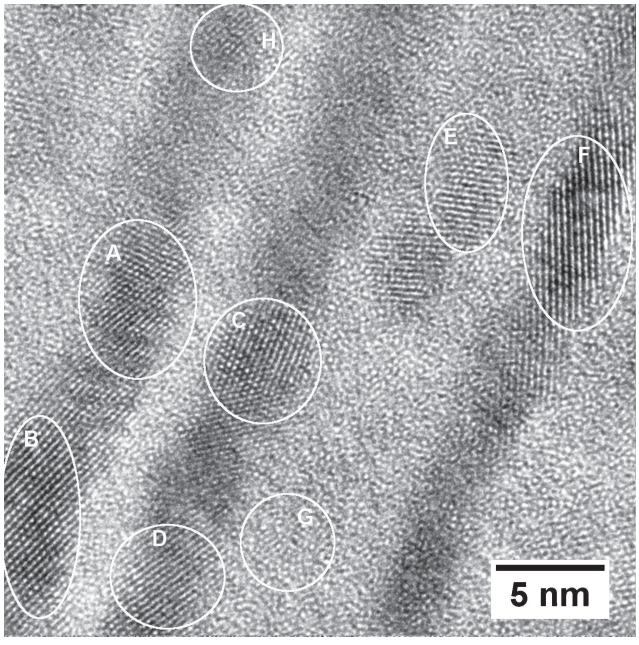

Figure 5. High-resolution lattice image from a multilayer region portion of the heat treated specimen. Lattice planes of ZrO_2 alone are imaged since the Al_2O_3 layers are amorphous. The layer boundaries are not distinct, t-ZrO_2 phases are observed to be separated by some amorphous regions.

and zirconia is less clear. The zirconia crystallite sizes (∼7–8 nm) are almost the same as the thickness of the zirconia layer perpendicular to the substrate. Regions corresponding to crystalline zirconia in figure 5 selected for analysis are labelled from A to H. Inter-planar spacings and in suitable cases inter-planar angles, measured on power spectra calculated from each of these regions showed that the crystalline areas in the zirconia layer can be indexed as tetragonal zirconia.

One such measurement is illustrated in figure 6, where a detailed view of the lattice structure of a crystallite in the zirconia layer is presented. The measured lattice spacing is 0.295 nm with an inter-planar angle of about ∼70°. These lattice planes correspond to (011) plane of tetragonal zirconia. Here, the white dots correspond to the atomic columns from the respective crystalline planes. Multislice simulation has been carried out along the [11–1] zone axis of t-ZrO_2 in support of the experimental results shown in the inset of figure 6. In the simulated image, the interplanar angle is found to be 70.3°, which matches the experimental results.

An important observation of this work is the stabilization of t-ZrO_2 of thickness 7–8 nm which is well in accordance with critical thickness reported for the free-standing nanocrystalline zirconia in literature.[12,14,15,18–22,32] In accordance with our earlier XRD-based studies,[34–36] the present HRTEM evidence shows conclusively that tetragonal ZrO_2 has been stabilized in the size range of 7–8 nm after heat treatment for the multilayer specimen containing 7-nm-thick ZrO_2 laminate. A combination of factors can be responsible for this. The tetragonal structure of zirconia has a unit cell volume that is less than half that of the monoclinic unit cell. Al_2O_3 has high elastic constant (390 GPa), which is almost twice that of ZrO_2.[37] The combination of large volume expansion required for tetragonal → monoclinic transformation in the presence of high modulus constraining layers would ensure stability of the tetragonal phase once formed during heat treatment. It is however, the inter-layer and intra-layer interface constraints that contribute significantly to phase stability at such small length scales.

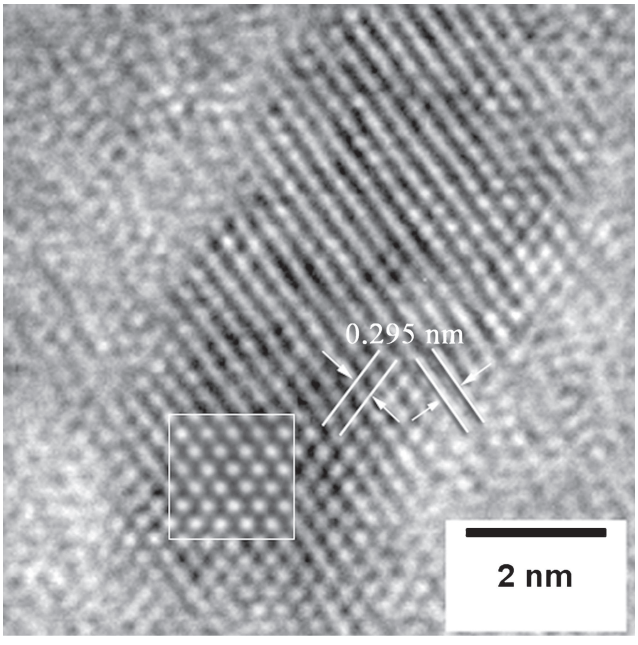

Figure 6. High-resolution lattice image from a zirconia nanocrystallite. The dimension of the crystallite in the perpendicular direction of the substrate is that of the layer width only. The lattice spacings are 0.295 nm with an interplanar angle of ∼70° corresponding to the (011) plane of t-ZrO_2. (inset) Simulated image of t-ZrO_2 along the [11−1] zone axis imaging the (011) planes.

The possibility for the formation of amorphous zones in the zirconia layers is another important finding of this study. The presence of such regions may indicate inter-mixing of alumina and zirconia leading to formation of zirconium aluminate phase. These non-crystalline zones are not a phase contrast imaging artefact has been checked by varying the objective lens defocus as well as by tilting the specimen. However, there is indication in literature, that this may indeed take place. It has been reported by Zhao *et al*[38,39] that intermixing of such phases (ZrO_2 and Al_2O_3) could lead to the formation of amorphous $ZrAl_xO_y$. Annealing at high temperatures could result in the initial stages of the nucleation of t-ZrO_2 which is also supported by the phase diagram.[40] It is interesting to note that, throughout the phase transformation process, the overall multilayer structure is maintained.

These observations are consistent with other experiments, including our own, where alumina layers have been replaced by ceria[41–47] or yttria.[48–54] In the ceria/zirconia multilayer system the zirconia nanocrystallites have been observed to be stabilized in the tetragonal phase even at room temperature, whereas the thermally annealed CeO_2/ZrO_2 multilayers at ∼1473 K shows the formation of solid solutions near the interfaces.[46] This is also evident from the equilibrium phase diagram.[55] The structural similarity and higher solubility of ceria in zirconia could possibly lead to the stabilization of the tetragonal structure in zirconia nanolaminate even at room temperature for CeO_2/ZrO_2 multilayers than those of Al_2O_3/ZrO_3 multilayers. On the other hand, the addition of Y_2O_3 to zirconia significantly promotes the diffusionless cubic phase transition in zirconia, stabilizing the high temperature phases down to room temperature. This transformation is facilitated at a faster rate because of the higher solubility and structural similarities of yttria and zirconia with negligible constraint by yttria.

Another important observation of the present study is the stabilization of the tetragonal phase and not the cubic phase of zirconia because of the annealing at the high temperature. This can be explained based on the coordination geometry associated with the oxygen ion vacancies with Zr^{4+} ions. Although the oxygen ion vacancies can be generated inside the ZrO_2 nanocrystals at the higher temperature but the same effect can also be obtained by replacing Zr^{4+} ion with trivalent cations. In literature, it has been reported that both oversized (e.g., Y^{3+}, Gd^{3+}) and undersized (e.g., Al^{3+}, Ga^{3+}) trivalent cations are effective for the stabilization of the tetragonal and cubic phases. The doped oversized cations favour the eight-fold coordination and allow associating the oxygen ion vacancies with the host Zr^{4+} cations. As a result

small as well as large concentration of oxygen ion vacancies associated with Zr^{4+} can be produced. Thus both tetragonal and cubic phases can be stabilized at room temperature by doping oversized cations. For doped undersized cations (Al^{3+} size = 0.0535 nm), as in the case of present work, they prefer the six-fold coordination and hence compete with the host Zr^{4+} cations (size = 0.0720 nm) for the oxygen vacancies. As a result only small concentrations of oxygen ion vacancies associated Zr^{4+} cations can be produced inspite of doping large amount undersized cations. Hence, only tetragonal phase can be stabilized at room temperature by doping undersized Al^{3+} ions in the zirconia nanocrystals.[10,11,56]

One of the objectives of this paper is also to study the ZrO_2 layer thickness on the stabilization of the high temperature tetragonal phase. For that particular purpose multilayers consisted of alternate layers of ZrO_2 and Al_2O_3 at different zirconia layer thicknesses (15 and 7 nm) has been synthesized keeping the thickness of the alumina layers same. Further structural characterization suggests that for the 15-nm-thick ZrO_2 layers the majority of the phases are of monoclinic structure whereas for the 7-nm-thick ZrO_2 layers, the nanocrystallites has been stabilized as tetragonal structure in the as-deposited condition. This is also justified based on the literature reports where the surface energy theory clearly suggests a critical size of 10 nm below which the high temperature tetragonal structure is thermodynamically stable at room temperature.[18–22]

The phase transformations among monoclinic, tetragonal and amorphous polymorphs[57] have a significant implication in designing novel ZrO_2-based nanostructures for a wide range of technological applications. The present work has also highlighted some of the issues related to the phase and chemical stability of the multilayers in the as-deposited and in the high temperature annealed conditions.

4. Conclusions

The HRTEM characterization of the structure and morphology of alumina/zirconia multilayers deposited through PLD have been carried out to study the phase stability of multilayers as a function of temperature. The study has highlighted the phase stability of alumina/zirconia multilayer in the as-deposited and annealed conditions. The results show that the heat-treated zirconia layers contain tetragonal nanocrystallites which remain stable at room temperature. However, the alumina layer remained in amorphous state up to the high temperature annealing of 1473 K. The stabilization of high temperature tetragonal phase at room temperature is supposed to be due to the addition of alumina in the multilayers.

One of the consequences of the interdiffusion of alumina and zirconia in the nm scale is the possible formation of amorphous intermixed zones which affects the crystalline uniformity of the corresponding nanolayer. The possible formation of the amorphous phases may also lead to the variation of the stoichiometry in the film.

Acknowledgements

We acknowledge the support and encouragement from Dr M Vijayalakshmi, Associate Director, Physical Metallurgy Group, Dr T Jayakumar, Director, Metallurgy and Materials Group and Dr P R Vasudeva Rao, Director, IGCAR.

References

1. Wright P K and Evans A G 1999 *Solid State Mater. Sci.* **4** 255
2. Zhou X, Balachov I and Macdonald D D 1998 *Corros. Sci*. **40** 1349
3. Gong W L, Lutze W and Ewing R C 2000 *J. Nucl. Mater.* **277** 239
4. Duparre A, Welsch E, Walther H, Kaiser N, Muller H, Hacker E, Lauth H, Meyer J and Weissbrodt P 1990 *Thin Solid Films* **187** 275
5. Andritschky M, Cunha I and Alpium P 1997 *Surf. Coat. Technol.* **94–95** 144
6. Grain C F 1967 *J. Am. Ceram. Soc*. **50** 288
7. Scott H G 1975 *J. Mater. Sci.* **10** 1527
8. Stubican V S and Ray S P 1977 *J. Am. Ceram. Soc.* **60** 534
9. Christensen A and Carter E 1998 *Phys. Rev. B* **58** 8050
10. Shukla S and Seal S 2005 *Int. Mater. Rev.* **50** 1
11. Li P, Chen I-W and Penner-Hahn J E 1994 *J. Am. Ceram. Soc.* **77** 118
12. Garvie R C 1965 *J. Phys. Chem.* **69** 1238
13. Lange F F, Green D J, Heuer A H and Hobbs L W (eds) 1981 *Advances in ceramics, vol. 3, science and technology of zirconia* (Columbus, OH: American Ceramic Society) p 217
14. Evans A G, Burlingame N, Drory M and Kriven W M 1981 *Acta Metall*. **29** 447
15. Aita C R, Wiggins M D, Whig R, Scanlan C M and Gajdardziska-Josifovska M 1996 *J. Appl. Phys.* **79** 1176
16. Garvie R C 1978 *J. Phys. Chem.* **82** 218
17. Kresse G and Furthmuller J 1996 *Phys. Rev. B* **54** 11169
18. Chatry M, Henry M and Livage J 1994 *Mater. Res. Bull.* **29** 517
19. Urlacher C, Dumas J, Serughetti J, Mugneir J and Munoz M 1997 *J. Sol–Gel Sci. Technol.* **8** 999
20. Xin B, Duan L and Xie Y 2000 *J. Am. Ceram. Soc.* **83** 1077
21. Noh H-J, Seo D-S, Kim H and Li J-K 2003 *Mater. Lett.* **57** 2425
22. Nitsche R, Rodewald M, Skandan G, Fuess H and Hahn H 1997 *Nanostruct. Mater.* **6** 679
23. Shanmugavelayathamn G, Shoji Y and Kobayashi A 2006 *Vaccum* **80** 1336
24. Bermejo R, Torres Y, Baudin C, Sanchez-Herencia A J, Pascual J, Anglada M and Llanes L 2007 *J. Eur. Ceram. Soc.* **27** 1443
25. Schofield M A, Aita C R, Rice P M and Gajdardziska-Josifovska M 1998 *Thin Solid Films* **326** 106
26. Schofield M A, Aita C R, Rice P M and Gajdardziska-Josifovska M 1998 *Thin Solid Films* **326** 117
27. Teixeira V, Monteiro J, Duarte J and Portinha A 2002 *Vaccum* **67** 477

28. Gao P, Meng L J, Dos Santos M P, Teixeira V and Andritschky M 2002 *Vaccum* **64** 477
29. Leushake U, Krell T, Schulz U, Peters M, Kaysser W A and Rabin B H 1997 *Surf. Coat. Technol*. **94–95** 131
30. Caricato A P, Di Cristoforo A, Fernandaz M, Leggieri G, Luches A, Majni G, Martino M and Mengucci P 2003 *Appl. Surf. Sci.* **208–209** 632
31. Hirschauer B, Chiaia G, GÖthelid M and Karlsson U O 1999 *Thin Solid Films* **348** 3
32. Lange F F 1982 *J. Mater. Sci*. **17** 225
33. Limarga Andi M, Widjaja Sujano and Yip Tick Hon 2005 *Surf. Coat. Technol.* **197** 93
34. Balakrishnan G, Kuppusami P, Sairam T N, Thirumurugesan R, Mohandas E and Sastikumar D 2009 *J. Nanosci. Nanotechnol.* **9** 1
35. Balakrishnan G, Murugesan S, Ghosh C, Kuppusami P, Divakar R, Mohandas E and Sastikumar D 2009 *Proceedings of SPIE, vol. 7404, 74040P, Nanostructured thin films II*, San Diego, CA, USA, 5 August 2009
36. Balakrishnan G, Kuppusami P, Murugesan S, Ghosh C, Divakar R, Mohandas E and Sastikumar D 2012 *Mater. Chem. Phys.* **133** 299
37. Scanlan C M, Gaijdardziska-Josifovska M and Aita C R 1994 *Appl. Phys. Lett.* **64** 3548
38. Zhao C, Richard O, Bender H, Caymax M, De Gendt S, Heyns M, Young E, Roebben G, Van Der Biest O and Haukka S 2002 *Appl. Phys. Lett*. **80** 2374
39. Zhao C, Richard O, Young E, Bender H, Roebben G, Haukka S, De Gendt S, Houssa M, Carter R, Tsai W, Van Der Biest O and Heyns M 2002 *J. Non-Cryst. Solids* **303** 144
40. Lakiza S N and Lopato L M 1997 *J. Am. Ceram. Soc.* **80** 893
41. Wang C M, Azad S, Shutthanandan V, McCready D E, Peden C H F, Saraf L and Thevuthasan S 2005 *Acta Mater*. **53** 1921
42. Yashima M, Sasaki S, Yamaguchi Y, Kakihana M, Yoshimura M and Mori T 1998 *Appl. Phys. Lett.* **72** 182
43. Yashima M, Arashi H, Kakihana M and Yoshimura M 1994 *J. Am. Ceram. Soc.* **77** 1067
44. Sasaki T, Ukyo Y, Kuroda K, Arai S and Saka H 2005 *Mater. Sci. Forum* **475–479** 1351
45. Yashima M 2009 *J. Phys. Chem. C.* **113** 12658
46. Ghosh Chanchal, Divakar R, Balakrishnan G, Kuppusami P, Mohandas E and Sastikumar D 2010 *IIM NMD-ATM 2010*, Bangalore, India, November 14–16, 2010
47. Balakrishnan G, Kuppusami P, Murugesan S, Ghosh Chanchal, Divakar R, Mohandas E and Sastikumar D 2011 *Trans. Ind. Inst. Met.* **64** 297
48. Appel C C, Botton G A, Horsewell A and Stobbs W M 1999 *J. Am. Ceram. Soc* **82** 429
49. Chaim R, Ruhle M and Heuer A H 1985 *J. Am. Ceram. Soc.* **68** 427
50. Lanteri V, Chaim R and Heuer A H 1986 *J. Am. Ceram. Soc.* **69** C-258
51. Zhou Y, Lei T C and Sakuma T 1991 *J. Am. Ceram. Soc.* **74** 633
52. Mengucci P, Barucca G, Caricato A P, Di Cristoforo A, Leggieri G, Luches A and Majnia G 2005 *Thin Solid Films* **478** 125
53. Piascik J R, Zhang Q, Bower C A, Thompson J Y and Stoner B R 2007 *J. Mater. Res.* **22** 1105
54. Mishra Maneesha, Kuppusami P, Reddy V R, Singh Akash, Chinnamma G, Ghosh Chanchal, Divakar R and Mohandas E 2013 *J. Nanosci. Lett.* **3** 4
55. Duwez P and Odell F 1950 *J. Am. Ceram. Soc*. **33** 280
56. Zuo Y, Kim S W, Masui T and Imanaka N 2014 *ECS J. Solid State Sci. Technol.* **3** R79
57. Lian J, Zhang J, Namavar F, Zhang Y, Lu F, Haider H, Garvin K, Weber W J and Ewing R C 2009 *Nanotechnology* **20** 245303